Universality Classes in Constrained Crack Growth

Knut S. Gjerden,* Arne Stormo,† and Alex Hansen‡

Department of Physics, Norwegian University of Science and Technology, N-7491 Trondheim, Norway

(Received 11 January 2013; revised manuscript received 29 July 2013; published 24 September 2013)

Based on an extension of the fiber bundle model we investigate numerically the motion of a crack front through a weak plane separating a soft and an infinitely stiff block. We find that there are two regimes. At large scales the motion is consistent with the pinned elastic line model and we find a roughness exponent equal to 0.39 ± 0.04 characterizing it. At smaller scales, coalescence of holes dominates the motion, giving a roughness exponent consistent with $2/3$, the gradient percolation value. The length of the crack front is fractal in this regime. Its fractal dimension is 1.77 ± 0.02, consistent with the hull of percolation clusters, $7/4$. This suggests that the crack front is described by two universality classes: on large scales, the pinned elastic line one and on small scales, the percolation universality class.

DOI: 10.1103/PhysRevLett.111.135502 PACS numbers: 62.20.mt, 46.50.+a, 68.35.Ct

Schmittbuhl and Måløy [1] were the first to study experimentally the roughness of a crack front moving along a weak plane under mode I loading. By sintering two sand-blasted plexiglass plates together and then plying them apart from one edge, they were able to follow the motion of the crack front moving along the sintered boundary. The rough crack front turned out to be self-affine; i.e., its height-height correlation function $\langle (h(x + \Delta x) - h(x))^2 \rangle$ scaled as $|\Delta x|^{\zeta}$, where ζ is the roughness exponent. $h(x)$ is the position of the crack front with respect to a base line orthogonal to the average crack growth direction and x is the coordinate along this base line. The roughness exponent was found to be $\zeta = 0.55 \pm 0.05$. A couple of years before, Schmittbuhl *et al*. [2] studied numerically a model of such constrained crack growth based on regarding the motion of the crack front as that of a pinned elastic line, the fluctuating line model. This top down approach was based on an earlier idea by Bouchaud *et al.* [3]. The conclusion of Schmittbuhl *et al*. was that the front should be self-affine, with a roughness exponent $\zeta = 0.35 \pm 0.05$. This value was refined to 0.388 ± 0.002 by Rosso and Krauth [4]. The large discrepancy between the numerical and experimental results—the latter having been refined to $\zeta = 0.63 \pm 0.03$ by improving the statistical analysis [5]—spurred a lively quest for an explanation that only today seems to converge towards a satisfactory understanding of the underlying physics, see, e.g., [6,7] for a review.

A different, bottom-up approach to the motion of the crack front was put forward by Schmittbuhl, Hansen, and Batrouni [8], based on a fiber bundle model [9] connected to a soft clamp [10]. In this model, the crack front is an emergent property. The underlying idea here was that the crack front does not advance due to a competition between effective elastic forces and pinning forces at the front, but by *coalescence* of damage in front of the crack with the advancing crack itself. Such an idea had been put forward in a more general context by Bouchaud *et al.* [11] the year before. Schmittbuhl, Hansen, and Batrouni found a roughness exponent of $\zeta = 0.60 \pm 0.05$, which is consistent with the experimental results.

Recently, Santucci *et al.* [12] reanalyzed data from a number of earlier studies, including [5], finding that the crack front has *two scaling regimes:* one small-scale regime described by a roughness exponent $\zeta_- = 0.60 \pm 0.05$ and a large-scale regime described by a roughness exponent $\zeta_+ = 0.35 \pm 0.05$.

We suggest in this Letter that there are indeed two competing mechanisms involved in generating the scaling properties seen in the roughness of the crack front: on small scales coalescence dominates, whereas on large scales, the fluctuating line picture is correct. There is a crossover between the regimes where either of the two mechanisms dominate associated with a well-defined crossover length scale.

Our numerical work strongly suggest that the coalescence mechanism seen at small scales is controlled by the ordinary percolation critical point, leading to percolation exponents. This is in contrast to Schmittbuhl, Hansen, and Batrouni [8] who suggested a new percolationlike universality class, but consistent with recent theoretical work on fracture in the fuse model [13].

We note an earlier attempt at explaining the two scaling regimes seen in Ref. [12] based solely on the fluctuating line model [14]. Here, Laurson, Santucci, and Zapperi [14] relate the crossover to the Larkin length scale of the crack front [15]. This is in this context the length scale at which the roughness of the front is comparable to the correlation length inherent to the pinning disorder. In our model, the large scale fluctuating line picture is an *emergent* property as is the small-scale percolationlike behavior.

$L \times L$ elastic fibers are placed in a square lattice between two clamps. One clamp is infinitely stiff whereas the other has a finite Young modulus E and a Poisson ratio ν. All fibers are equally long and have the same elastic constant k. We measure the position of the stiff clamp with respect to its position when all fibers carry zero force, D.

The force carried by the fiber at position (i, j), where i and j are coordinates in a Cartesian coordinate system oriented along the edges of the system, is then

$$f_{(i,j)} = -k(u_{(i,j)} - D), \tag{1}$$

where $u_{(i,j)}$ is the fiber's elongation. The fibers redistribute the forces they carry through the response of the clamp with finite elasticity. The redistribution is accomplished by using the Green function connecting the force $f_{(m,n)}$ acting on the clamp from fiber (m, n) with the deformation $u_{(i,j)}$ at fiber (i, j), [16]

$$u_{(i,j)} = \sum_{(m,n)} G_{(i,j),(m,n)} f_{(m,n)}, \tag{2a}$$

$$G_{(i,j),(m,n)} = \frac{1-\nu^2}{\pi E a^2} \int_{-a/2}^{a/2} dx \times \int_{-a/2}^{a/2} dy \frac{1}{|\vec{r}_{(i,j)} - \vec{r}_{(m+x,n+y)}|}. \tag{2b}$$

where a is the distance between neighboring fibers. $\vec{r}_{(i,j)} - \vec{r}_{(m,n)}$ is the distance between fibers (i, j) and (m, n) and the integration runs over the $a \times a$ square around fiber (m, n). This equation set is solved using a Fourier accelerated conjugate gradient method [17,18].

The Green function, Eq. (2b), is proportional to $(Ea)^{-1}$. The elastic constant of the fibers, k, must be proportional to a^2. The linear size of the system is aL. Hence, by changing the linear size of the system without changing the discretization a, we change $L \to \lambda L$ but leave (Ea) and k unchanged. If, on the other hand, we change the discretization without changing the linear size of the system, we simultaneously set $L \to \lambda L$, $(Ea) \to \lambda(Ea)$ and $k \to k/\lambda^2$. We define the scaled Young modulus $e = (Ea)/L$. Hence, changing e without changing k is equivalent to changing L—and hence the linear size of the system—while keeping the elastic properties of the system constant [19].

The fibers are broken by using the quasistatic approach [20]: we assign to each fiber (i, j) a threshold value $t_{(i,j)}$. They are then broken one at a time by each time identifying $\max_{(i,j)}(f_{(i,j)}/t_{(i,j)})$ for $D = 1$. This ratio is then used to read off the value D at which the next fiber breaks.

In the constrained crack growth experiments of Schmittbuhl and Måløy [1], the two sintered plexiglass plates were plied apart from one edge. In the numerical modeling of Schmittbuhl, Hansen, and Batrouni [8], an asymmetric loading was accomplished by introducing a linear gradient in D. We introduce a gradient in the threshold distribution, $t_{(i,j)} = gj + r_{(i,j)}$, where g is the gradient and $r_{(i,j)}$ is a random number drawn from a flat distribution on the unit interval. In the limit of large Young modulus E, this system becomes equivalent to the gradient percolation problem [21,22].

We implement the "conveyor belt" technique [23,24] where a new upper row of intact fibers is added and a lower row of broken fibers removed from the system at regular intervals. This makes it possible to follow the advancing crack front indefinitely; see [24].

Figure 1 shows two examples of typical crack fronts representative of a stiff (high $e = 0.8$) and a soft system (low $e = 2 \times 10^{-3}$). The crack front propagates upwards in the figure. A high e value is equivalent to observing the system on small scales and a low e value corresponds to large scales.

We identify the crack front by first eliminating all islands of surviving fibers behind it and all islands of failed fibers in front of it. We measure "time" n in terms of the number of failed fibers. After an initial period, the system settles into a steady state. We then record the position of the crack front $j = j(i, n = 0)$ after having set $n = 0$. We then define the position at later times $n > 0$ relative to this initial position, $h_i(n) = j(i, n) - j(i, n = 0)$. This is the same definition as was used by Schmittbuhl and Måløy [1]. The front as it has now been defined will contain overhangs. That is, there may be multiple values of $h_i(n)$ for the same i and n values. We only keep the largest $h_i(n)$; i.e., we implement the solid-on-solid (SOS) front. We define the average position of the front as $\langle h(n)\rangle = \sum_{i=1}^{L} h_i(n)/L$ and the front width as $w(n)^2 = \sum_{i=1}^{L}(h_i(n) - \langle h(n)\rangle)^2/L$.

We will in the following explore the model going from large to small values of the Young modulus E while keeping k fixed. As already discussed, this is equivalent to changing the system size L while keeping E fixed.

Further description of the model together with illustrative films have been added as Supplemental Material [25].

We analyze the fracture fronts in the following using the average wavelet coefficient (AWC) method [26,27]. We transform the front $h_i(n)$ using the Daubechies-4 wavelet, $h_i(n) \to w_{a,b}$ where a is scale and b is position (and we have suppressed the n dependency). We then average $|w_{a,b}|$ for each length scale a over position b, and if $h_i(n)$ is self-affine with a roughness exponent ζ, we have

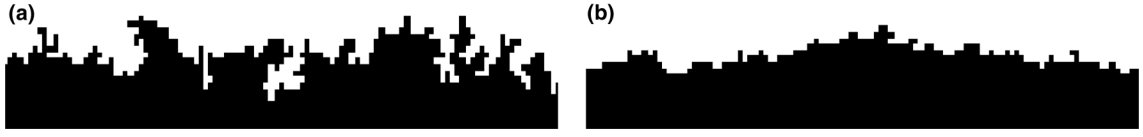

FIG. 1. Parts of the crack fronts obtained in the simulations. Black represents broken bonds and white represents unbroken bonds. To the left, (a) is a system with a high rescaled Young modulus e being driven forward (upward) primarily by coalescence with damage forming ahead of the crack front. (b) is a system with a low e. This system is being driven forward by overcoming pinning. Small $e = 2 \times 10^{-3}$ is equivalent to a larger system than one with a large $e = 0.8$.

$$W(a) = \langle |w_{a,b}| \rangle_b \sim a^{\zeta+1/2}. \quad (3)$$

We start by considering systems with small scaled Young modulus e. This is a soft system at small length scales—or equivalently, a stiffer system at large length scales. We set $e = 7.8125 \times 10^{-4}$. The fronts in this regime have an appearance as in Fig. 1(b). In Fig. 2, we plot the averaged wavelet coefficient $W(a)$ against the scale a. The data follow a power law, $W(a) \sim a^{0.39+1/2}$, leading to a roughness exponent of

$$\zeta_+ = 0.39 \pm 0.04, \quad (4)$$

entirely consistent with the large scale roughness exponent measured by Santucci *et al.* [12], $\zeta_+ = 0.35 \pm 0.05$.

We now turn to large scaled Young modulus, i.e., stiff systems—or, equivalently, softer systems on small length scales. Hence, fronts appear as in Fig. 1(a). We set in the following $e = 3.125$. The corresponding plot of averaged wavelet coefficient $W(a)$ vs scale a is shown in the inset in Fig. 3(a). The different curves correspond to different gradients g and L. Repeating the analysis of Sapoval, Rosso, and Gouyet [21] and Hansen *et al.* [28] for gradient percolation, we assume that the front has an isotropic correlation length ξ associated with it. This correlation length is related to the gradient through the relation $\xi \sim g^{-\nu/(1+\nu)} = g^{-4/7}$, where $\nu = 4/3$ is the percolation correlation length exponent. If the front is in the universality class of percolation, we expect data collapse in Fig. 3(a) by rescaling $W(a) \to W(a)/\xi = W(a)/g^{-6/7}$ and $a \to a/\xi = a/g^{-4/7}$. There are two distinct regions in the figure. For large values of $a/g^{-4/7}$, $W(a)/g^{-6/7}$ is independent of $a/g^{-4/7}$. Hence, the front has the character of uncorrelated noise. We will discuss this further on. For small $a/g^{-4/7}$, the data follow a power law. We show in the figure [Fig. 3(a)] a straight line with slope $7/6 = 2/3 + 1/2$. Hence, the data are consistent with the fronts being self-affine with

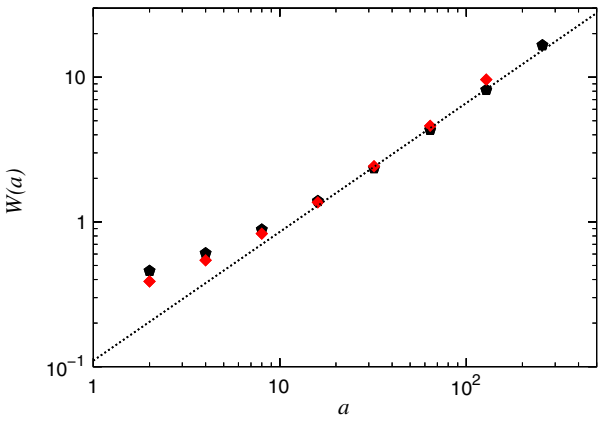

FIG. 2 (color online). Averaged wavelet coefficient $W(a)$ based on transforming h_i vs a for $e = 7.8125 \times 10^{-4}$, $L = 256$ ($g = 0.006\,25$, averaged over 4200 fronts), and $L = 512$ ($g = 0.003\,125$, averaged over 850 fronts). The slope of the straight line is $0.39 + 1/2$.

$$\zeta_- = 2/3, \quad (5)$$

consistent with gradient percolation [28] and with the experimental value of Santucci *et al.* [12], $\zeta_- = 0.60 \pm 0.05$.

In order to further the analysis, we follow the procedure in [28] by smoothening the fronts by removing the jumps due to the overhangs through the transformation

$$h_i(n) \to h_i^k(n) = \sum_{m=0}^{i} \mathrm{sgn}[h_{m+1}(n) - h_m(n)] \times |h_{m+1}(n) - h_m(n)|^k, \quad (6)$$

when $k \to 0$ [29]. Hence, all steps are equal to one in $h_i^0(n)$, all overhangs have been removed. We ensure by this

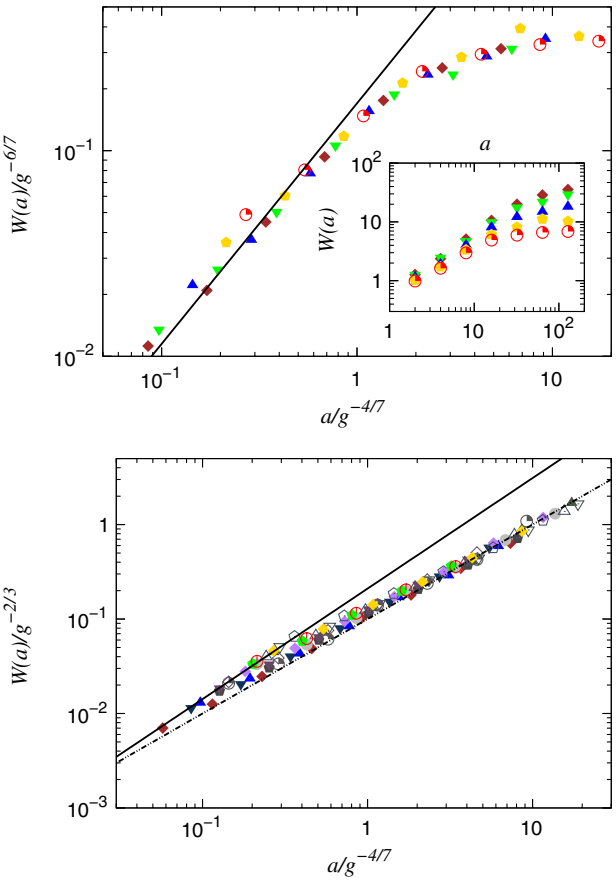

FIG. 3 (color online). (a) Averaged wavelet coefficients $W(a)$ of the SOS front h_i vs scale a. The straight line has slope $2/3 + 1/2 = 6/7$. The inset shows the unscaled data. The data are based on $e = 3.125$, $L = 256$ ($g = 0.004$, 0.005, 0.01, 0.02, and 0.03). (b) Average wavelet coefficients $W(a)$ of the SOS fronts h_i^0 where the overhangs have been removed. The long-dashed line has slope $2/3 + 1/2 = 6/7$ and the short-dashed line has slope $1/2 + 1/2 = 1$. In both (a) and (b), $\alpha = \beta = 4/7$. The data are based on $e = 3.125$, $L = 64$ ($g = 0.018$ and 0.02, averaged over 1426 fronts), $L = 128$ ($g = 0.008$, 0.01, 0.03, and 0.05, averaged over 100 to 500 fronts), $L = 256$ ($g = 0.004$, 0.005, 0.008, 0.01, 0.015, 0.02, 0.025, 0.03, and 0.035, averaged over 30 to 500 fronts), and $L = 512$ ($g = 0.002$, averaged over 50 fronts).

procedure that the scaling properties of the roughness are due to self-affinity and *not* due to the overhangs which are prevalent in this regime.

We plot in Fig. 3(b) the rescaled $W(a)/g^{-2/3}$ based on transforming h_i^0 vs the rescaled $a/g^{-4/7}$, following the analysis of Hansen *et al.* [28]. The two straight lines that have been added to the figure have slopes $2/3 + 1/2 = 7/6$ and $1/2 + 1/2 = 1$, respectively. On small scales, the fronts are then self-affine with a roughness exponent $\zeta_- = 2/3$—the gradient percolation value. On larger scales and with the overhangs removed, one would naively have expected to observe the fluctuating line regime characterized by a roughness exponent $\zeta_+ = 0.39$. However, by removing the overhangs, the effective roughness exponent one measures is $\max(1/2, \zeta_+)$, which in this case is $1/2$ [29]. Figure 3(b) then shows the crossover from a roughness exponent consistent with ordinary gradient percolation to a plain random walk exponent which is a result of the smoothening process.

Hence, the scaling properties seen on small scales are consistent with uncorrelated gradient percolation. This is in constrast to the analysis of Schmittbuhl, Hansen, and Batrouni [8], which suggested a correlated gradient percolation process.

Roughness exponents are notoriously difficult to measure. The data presented in Fig. 3 are not of sufficient quality to warrant firm conclusions on the small-scale universality class by themselves. We therefore measure the *fractal dimension* of the fronts. Leaving the SOS assumption, we now follow the front as shown in Fig. 1. The front has a length l. For small values of the scaled Young modulus e, there are no (or very few) overhangs and we expect l to be proportional to L: it is not fractal. However, for large e where overhangs are prevalent, we do expect it to be fractal. We assume that there is a correlation length ξ and that the front is fractal up to this scale. Hence, the length of the front l then scales as $l \sim \xi^{D_f}(L/\xi)$. From Sapoval, Rosso, and Gouyet [21], we know that $\xi \sim g^{-\nu/(1+\nu)}$. We now set $g = c/L$, where c is a constant. Hence, we find

$$l \sim L^{(\nu D_f + 1)/(\nu+1)} \sim L^{10/7}, \tag{7}$$

where $\nu = 4/3$ and $D_f = 7/4$ [22]. We show in Fig. 4, $l/L^{10/7}$ as a function of the scaled Young modulus, e. For large values of e, there is excellent data collapse. For small values of e, there is data collapse when l/L is plotted against e, see the insert of Fig. 4, indicating that the front is not fractal in this regime. We are seeing the crossover from the coalescence-dominated regime to the fluctuating line regime as e moves from large to smaller values. Since $e = E/L$, we may keep E fixed and change e by changing L. Hence, the coalescence regime is a small-scale regime whereas the fluctating line regime is a large-scale regime.

If we work backwards and search for the best scaling exponent to produce data collapse in Fig. 4, we find $l/L^{1.44}$.

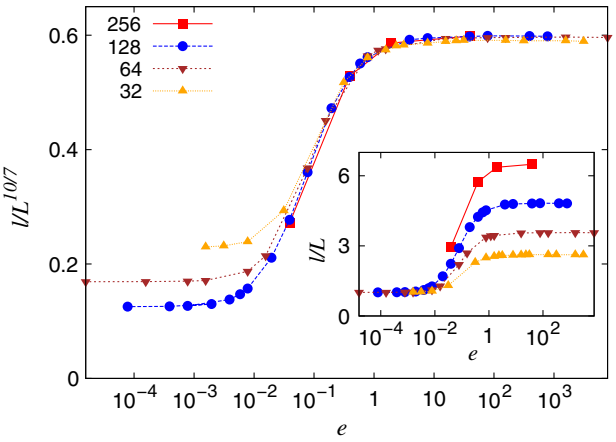

FIG. 4 (color online). Length of the fracture front l scaled by system size plotted against effective Young modulus e. The main figure shows data collapse for $l/L^{10/7}$ for large e values and the inset shows data collapse for small e values for l/L^1. We set $g = 1.6/L$. The data are based on 425 000 fronts for $L = 32$, 286 482 fronts for $L = 64$, 282 022 fronts for $L = 128$ and 32 117 fronts for $L = 256$.

This gives $D_f = 1.77 \pm 0.02$, consistent with the percolation value $7/4$.

We have through the use of a single bottom-up model based on the fiber bundle model with a soft clamp and a gradient in the breaking threshold, been able to identify two mechanisms by which the fracture front propagates. On small scales, it is coalescence of damage that dominates, whereas on large scales the front advances as described by the fluctuating line model. The coalescence regime is in the universality class of ordinary percolation.

We are grateful for discussions with D. Bonamy, K. J. Måløy, L. Ponson, and K. T. Tallakstad. We thank the Norwegian Research Council for financial support (Grant No. 177591/V30). Part of this work made use of the facilities of HECToR, the UK's national high performance computing service.

*knut.skogstrand.gjerden@gmail.com
†arne.stormo@gmail.com
‡alex.hansen@ntnu.no

[1] J. Schmittbuhl and K. J. Måløy, Phys. Rev. Lett. **78**, 3888 (1997).
[2] J. Schmittbuhl, S. Roux, J.-P. Vilotte, and K. J. Måløy, Phys. Rev. Lett. **74**, 1787 (1995).
[3] J. P. Bouchaud, E. Bouchaud, G. Lapasset, and J. Planès, Phys. Rev. Lett. **71**, 2240 (1993).
[4] A. Rosso and W. Krauth, Phys. Rev. E **65**, R025101 (2002).
[5] A. Delaplace, J. Schmittbuhl, and K. J. Måløy, Phys. Rev. E **60**, 1337 (1999).
[6] D. Bonamy, J. Phys. D: Appl. Phys. **42**, 214014 (2009).
[7] D. Bonamy and E. Bouchaud, Phys. Rep. **498**, 1 (2011).

[8] J. Schmittbuhl, A. Hansen, and G. G. Batrouni, Phys. Rev. Lett. **90**, 045505 (2003).
[9] S. Pradhan, A. Hansen, and B. K. Chakrabarti, Rev. Mod. Phys. **82**, 499 (2010).
[10] G. G. Batrouni, A. Hansen, and J. Schmittbuhl, Phys. Rev. E **65**, 036126 (2002).
[11] E. Bouchaud, J. P. Bouchaud, D. S. Fisher, S. Ramanathan, and J. R. Rice, J. Mech. Phys. Solids **50**, 1703 (2002).
[12] S. Santucci, M. Grob, R. Toussaint, J. Schmittbuhl, A. Hansen, and K. J. Måløy, Europhys. Lett. **92**, 44 001 (2010).
[13] A. Shekawat, S. Zapperi, and J. P. Sethna, Phys. Rev. Lett. **110**, 185505 (2013).
[14] L. Laurson, S. Santucci, and S. Zapperi, Phys. Rev. E **81**, 046116 (2010).
[15] A. I. Larkin and Y. N. Ovchinnikov, J. Low Temp. Phys. **34**, 409 (1979).
[16] K. L. Johnson, *Contact Mechanics* (Cambridge University Press, Cambridge, England, 1985).
[17] G. G. Batrouni, A. Hansen, and M. Nelkin, Phys. Rev. Lett. **57**, 1336 (1986).
[18] G. G. Batrouni and A. Hansen, J. Stat. Phys. **52**, 747 (1988).
[19] A. Stormo, K. S. Gjerden, and A. Hansen, Phys. Rev. E **86**, R025101 (2012).
[20] A. Hansen, Comput. Sci. Eng. **7**, 90 (2005).
[21] B. Sapoval, M. Rosso, and J.-F. Gouyet, J. Phys. Lett. **46**, 149 (1985).
[22] J.-F. Gouyet and M. Rosso, Physica (Amsterdam) **357A**, 86 (2005).
[23] A. Delaplace, S. Roux, and G. Pijaudier-Cabot, J. Eng. Mech. **127**, 646 (2001).
[24] K. S. Gjerden, A. Stormo, and A. Hansen, J. Phys: Conf. Series **402**, 012039 (2012).
[25] See Supplemental Material at http://link.aps.org/supplemental/10.1103/PhysRevLett.111.135502 for a brief description of the model and films showing the motion of the fracture front in a soft system (or equivalently, on large scale) and in a stiff system (or equivalently, on small scale) with or without the fibers failing in front of the front shown. The latter makes the fracture front stand out.
[26] A. R. Mehrabi, H. Rassamdana, and M. Sahimi, Phys. Rev. E **56**, 712 (1997).
[27] I. Simonsen, A. Hansen, and O. M. Nes, Phys. Rev. E **58**, 2779 (1998).
[28] A. Hansen, G. G. Batrouni, T. Ramstad, and J. Schmittbuhl, Phys. Rev. E **75**, 030102 (2007).
[29] J. Ø. H. Bakke and A. Hansen, Phys. Rev. E **76**, 031136 (2007).